Structural changes of ZrO_2-CeO_2 solid solutions around the monoclinic-tetragonal phase boundary

Masatomo Yashima
Research Laboratory of Engineering Materials, Tokyo Institute of Technology, 4259, Nagatsuta, Midori-ku, Yokohama, 226, Japan

Teruo Hirose
Department of Industrial Chemistry, College of Science and Technology, Meiji University, Higashi-mita 1-1-1, Kawasaki, 214, Japan

Susumu Katano
Department of Materials Science and Engineering, Japan Atomic Energy Research Institute, Tokai, Ibaraki, 319-11, Japan

Yasuo Suzuki
Department of Industrial Chemistry, Faculty of Science and Technology, Meiji University, Higashi-mita 1-1-1, Kawasaki, 214, Japan

Masato Kakihana and Masahiro Yoshimura
Research Laboratory of Engineering Materials, Tokyo Institute of Technology, 4259, Nagatsuta, Midori-ku, Yokohama, 226, Japan
(Received 22 August 1994; revised manuscript received 12 December 1994)

High-resolution neutron-diffraction experiments have been performed to study the structural changes of ZrO_2 induced by CeO_2 doping. The crystal structures of monoclinic [$P2_1/c$, $Z=4$] and tetragonal [$P4_2/nmc$, $Z=2$] phases for ZrO_2–X mol % CeO_2 ($X=0$, 2, 5, 8, 10, 12, and 15) have been refined by the Rietveld analysis of the diffraction patterns measured at 298 K. The unit-cell parameters change anisotropically with an increase of CeO_2 content X. In the monoclinic phase a_m and c_m increase considerably while b_m shows a rather small increase with increasing X where the suffix m denotes the monoclinic phase. The angle β_m decreases with increasing X. The thermal ellipsoids also show large anisotropies, which correlate strongly with the directions of the movements of oxygen ions during the phase transition. The unit-cell parameters and the atomic positions discontinuously change during the monoclinic-tetragonal phase change. The crystal structure of monoclinic phase approaches that of tetragonal phase with an increase of X: (1) the length of a_m approaches that of b_m with increasing X, (2) the angle β_m decreases with X, and (3) all positional parameters of the monoclinic phase approach those of the tetragonal structure.

I. INTRODUCTION

Zirconia ceramics such as ZrO_2-CeO_2, ZrO_2-Y_2O_3, and ZrO_2-CaO are attractive materials as structural ceramics with high toughness, fuel cells, oxygen sensors, and refractories. Their physical and chemical properties relating to such uses are strongly dependent on the crystal structures, dopant concentration, temperature, and microstructures. A temperature-composition phase diagram of the ZrO_2-CeO_2 system is shown in Fig. 1.[1–5] Undoped zirconia (ZrO_2) has three solid polymorphisms of monoclinic, tetragonal, and cubic phases at atmospheric pressure.[6] The coordination polyhedra of the polymorphs are schematically shown in Fig. 2. The low-temperature stable monoclinic phase of ZrO_2 (space group $P2_1/c$) (Refs. 7 and 8) martensitically transforms into the tetragonal phase (space group $P4_2/nmc$) (Ref. 9) at about 1500 K,[10,11] and then a phase transition occurs from this tetragonal phase to a cubic fluorite-type structure (space group $Fm3m$) above 2560 K.[12] Both monoclinic and tetragonal phases have distorted fluorite structures (Fig. 2),[8] and the phase transitions among them are diffusionless in nature. On the basis of a geometrical comparison of the monoclinic and tetragonal structures, Smith and Newkirk[8] proposed possible atomic displacements during the phase transition in undoped ZrO_2, and their proposal was later supported by high-temperature neutron powder diffraction.[10] During this diffusionless phase transition, the oxygen O(1) has an important role, because the longest shift in the phase change should be the movement of the O(1) atom attached to the ZrO_7 group. Its coordination number changes from 3 (monoclinic) to 4 (tetragonal) as shown in Fig. 2.

Doping of an oxide such as CeO_2, Y_2O_3, and CaO into ZrO_2 extremely improves its mechanical and electrical properties such as toughness, strength, thermal-shock resistance, and ionic conductivity. The toughness of the ceria-doped zirconia ceramics (ZrO_2-X mol % $CeO_2=Zr_{1-X/100}Ce_{X/100}O_2$), for example, is considerably higher than those of undoped or yttria-doped ones (ZrO_2 and ZrO_2-Y_2O_3).[13–16] These properties can be correlated with the stabilization of high-temperature tetragonal and cubic phases in the lower-temperature region (Fig. 1). The diffusionless phase changes are described by the metastable phase boundaries as T_0^{t-m} (dashed lines in Fig. 1),[1,2,6,17,18] where the free energy of the tetragonal phase G_t equals that of the monoclinic phase G_m at a temperature T_0^{t-m}. High toughness of the doped zirconia is mainly ascribed to the stress-induced tetragonal-to-monoclinic phase transformation.[19,20] Therefore the

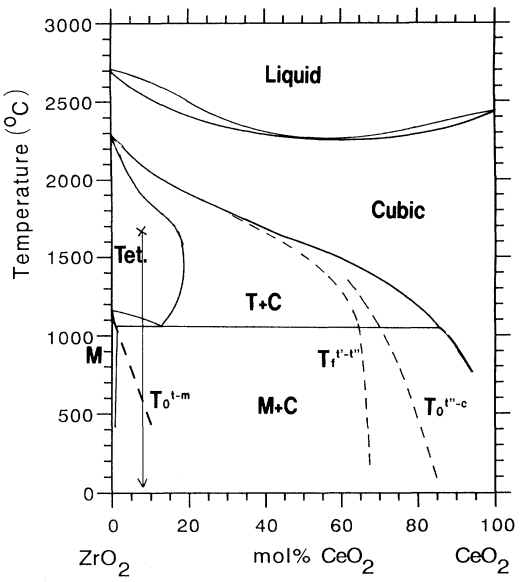

FIG. 1. Metastable and stable phase diagrams in the ZrO_2-CeO_2 system (Refs. 1 and 2). Solid lines are stable boundaries, and dashed ones for metastable. For a given composition, the $T_0^{t''-c}$ is defined as the temperature where the free energies of cubic and t'' forms are equal. The t'' form is a tetragonal phase where the axial ratio is unity, while the t' form is that whose c axis value is larger than the a axis one. These diffusionlessly formed metastable t' and t'' are conveniently distinguished from the diffusionally precipitated t form, although these three forms have the same crystal structure. The $T_f^{t'-t''}$ denotes the finishing point of the t'-to-t'' transformation, which was referred to $T_f^{t\to c}$ in Ref. 2.

transformation and phase change have been extensively studied by many researchers.[2,13–16,21–31]

Some previous work has studied the unit-cell parameters of the CeO_2-doped ZrO_2 from some peak positions observed in ordinary x-ray powder diffraction patterns.[4,13,27,31] However, these measurements are not highly accurate for the monoclinic phase because of the complexity of the powder diffraction patterns.[21] An unresolved issue is the compositional dependence of the unit-cell parameters around the monoclinic-tetragonal phase boundary.

The temperature dependence of the positional parameters of O(1) around the monoclinic-tetragonal transition point is important, because O(1) shows the longest movement during the transition.[8,10] Results of high-temperature neutron powder diffraction on undoped ZrO_2 (Ref. 10) seem to show that the positional parameters of this oxygen, x[O(1)] and y[O(1)], remain almost unchanged (apart a little from 0) with an increase of temperature above 1500 K. It is interesting to compare the monoclinic-tetragonal phase transition induced by CeO_2 doping with that under high temperature. However, the CeO_2 compositional dependence of the oxygen position is not known yet. A second unresolved issue concerns the atomic positional changes in the ZrO_2-CeO_2 solid solutions.

In the present study, high-resolution neutron diffraction is utilized both to quantify the oxygen position and to investigate the structural change with the help of the relatively large scattering length of oxygen in neutron diffraction. Rietveld refinements[32–34] of the high-resolution diffraction data,[35,36] which have a much higher resolving power for analyzing the complicated patterns of the monoclinic phase, are performed in the present study. We focus our attention on the compositional dependence of the oxygen positions and the unit-cell parameters around the monoclinic-tetragonal phase boundary.

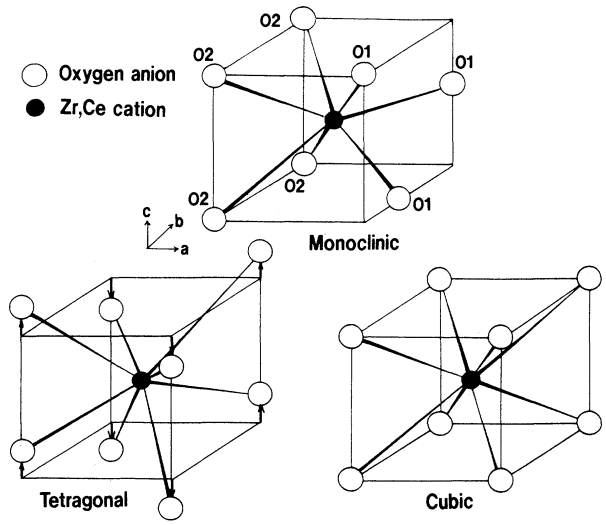

FIG. 2. Schematic cation coordination polyhedra in monoclinic, tetragonal, and cubic zirconias.

II. EXPERIMENTS AND DATA ANALYSIS

A. Sample preparation

The samples used for data collection were all prepared from commercially available zirconia containing a few amounts of hafnia that comes from raw materials (hafnium dioxide, HfO_2, 1.98 wt. % in ZrO_2). The starting materials were high-purity zirconia [Tosoh Co. Ltd., Tokyo, Japan, 99.9%, (97.9 wt. % ZrO_2+1.98 wt. % HfO_2), grade UPZ-200] and ceria (CeO_2, Shin-Etsu Chemicals Co. Ltd., Tokyo, Japan, 99.9%) powders. They were manually mixed as methanol slurries or dried powders in an agate mortar with a pestle for 3 h. The mixed powder was pressed into pellets (20 mm in diameter and 10–20 mm in height) by hand and then isostatically pressed at about 200 MPa. The pellets were fired at 1650 °C in air for 5 h in an electric furnace with $MoSi_2$ heaters, where the heating and cooling rates were 10 °C/min. Since the monoclinic phase forms through a diffusionless phase transition below T_0^{t-m} [arrow in Fig. 1 (Ref. 2)] from the tetragonal single-phase material (× in Fig. 1), we can investigate the crystal structures of compositionally homogeneous samples. Sintered products were white, indicating no oxygen vacancies at room temperatures, which might occur at high temperatures. Sintered materials were crushed into powders in an alumina mortar to measure the powder diffraction.

B. X-ray-diffraction measurement

X-ray powder diffraction was used to determine the lattice parameter of the ZrO_2-15 mol% CeO_2 sample. The sample was well mixed with an internal Si powder standard ($a_0 = 5.43094$ Å, 99.999%) for angular calibration. The x-ray-diffraction profiles of the mixed samples were collected with an x-ray diffractometer (MXP^{3VA}, MAC Science Co. Ltd., Tokyo, Japan) under the following experimental conditions: tube generated Cu $K\alpha$ radiation, curved graphite diffracted-beam monochromator, goniometer radius = 185 mm, divergence slit = 1°, antiscatter slit = 1°, receiving slit = 0.15 mm, NaI (Tl) scintillation counter, step-scan mode, step width = 0.02° in 2θ, fixed time = 5 s, and 2θ range = 68°–150°. Individual profile fits were performed for the powder data using a profile-fitting program PRO-FIT.[37] The peaks were fitted with a Pearson VII type function.[37]

C. Neutron-diffraction measurements

The powders were placed in a 10-mm outside diameter 50 mm vanadium holder with a wall thickness of 0.05 mm. Neutron-diffraction data for all samples were collected at 298 K with the high-resolution powder diffractometer (HRPD) at the JRR-3M of the Japan Atomic Energy Research Institute.[35,36,38] The HRPD is an ILL-D2B type diffractometer with a fine collimation system using 64 detectors placed at every 2.5° of the diffraction angle.[35,36] A neutron beam was monochromatized by the (311) plane of a Ge monochromator. The profile data were measured by scanning at intervals of 0.05° in the 2θ range of 5°–165°. The counting time was almost 12 or 21.6 min/points (10 or 18 h for a complete scan). The wavelength of the neutron beam was refined to be 1.8236 ±2 Å using the lattice parameter of ZrO_2-15 mol% CeO_2 by the method described before.[39]

The structural refinements were performed by a Rietveld analysis program RIETAN.[33,34] The peak shape was assumed to be a modified pseudo-Voigt function with asymmetry. The background of each profile was approximated by a six-parameter polynomial in $2\theta^n$, where n is a value from 0 to 5. The refinements were carried out with anisotropic atomic thermal parameters β_{ij} (Table I).

III. RESULTS AND DISCUSSION

The refinements for the ZrO_2-X mol% CeO_2 solid solutions were successfully performed by the monoclinic structure [$P2_1/c$, $Z=4$ (Refs. 7 and 8)] for $X=0,2,5,8$ by the tetragonal structure [$P4_2/nmc$, $Z=2$ (Ref. 9)] for $Z=15$ and by their mixtures for $X=10$ and 12 (Table I). No other phases were detected for all samples studied.

A. Unit-cell parameters

The unit-cell parameters of the monoclinic and tetragonal phases, a_m, c_m, $\sqrt{2}a_t$, and c_t, increase and the β_m angle decreases with an increase of CeO_2 content X (Figs. 3 and 4). The lattice parameter b_m increases in the compositional range of $0 \le X \le 8$ mol% CeO_2, but decreases a little at $10 \le X \le 12$ with an increase of X (Fig. 3). In consequence, the length of a_m approaches that of b_m. The unit-cell volumes of both monoclinic and tetragonal phases increase with increasing of X as seen in Fig. 5. These increases in unit-cell volumes are ascribed to the substitution by the larger-sized Ce^{4+} ion (the effective ionic radius is 0.97 Å for eightfold coordination[40]) for the smaller host Zr^{4+} (0.84 Å for eightfold coordination[40]).[41] These data of unit-cell parameters show good agreement with those in the previous works (Figs. 3–5).[4,27]

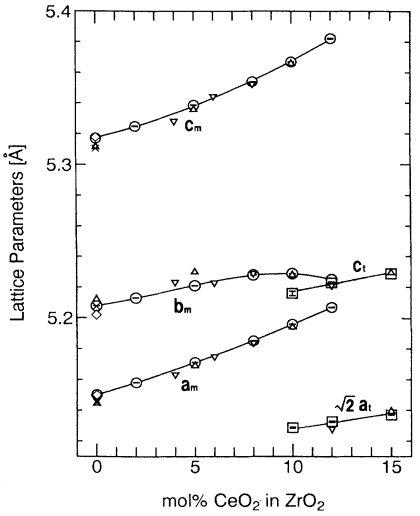

FIG. 3. Variation of the unit-cell parameters a_m, b_m, c_m, $\sqrt{2}a_t$, and c_t with the CeO_2 content: ○, present work (monoclinic phase); □, present work (tetragonal phase); △, Tani *et al.* (Ref. 4); ▽, Urabe *et al.* (Ref. 27); ◇; Frey *et al.* (Ref. 10); ×, Smith and Newkirk (Ref. 8).

The fracture toughness enhancement ΔK_{IC} by the tetragonal-to-monoclinic phase transition in Ce-doped tetragonal zirconia ceramics with fine grains of submicrometer is expressed as[20,42]

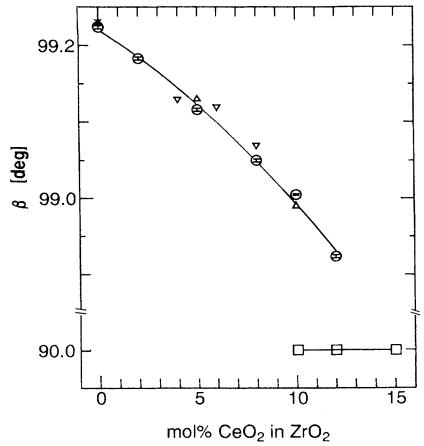

FIG. 4. Variation of the unit-cell parameter β_m with the CeO_2 content: ○, present work (monoclinic phase); □, present work (tetragonal phase); △, Tani *et al.* (Ref. 4); ▽, Urabe *et al.* (Ref. 27); ◇, Frey *et al.* (Ref. 10); ×, Smith and Newkirk (Ref. 8).

TABLE I. Summary of neutron-diffraction data refinement for ZrO_2-X mol % CeO_2 solid solutions. Standard Rietveld analysis agreement index (Ref. 46).

X of X mol % CeO_2	0	2	5	8	10		12		15
Space group	$P2_1/c$	$P2_1/c$	$P2_1/c$	$P2_1/c$	$P2_1/c$	$P4_2/nmc$	$P2_1/c$	$P4_2/nmc$	$P4_2/nmc$
a (Å)	5.1501(2)	5.1581(1)	5.1711(1)	5.1851(1)	5.1957(1)	3.6296(7)	5.2068(2)	3.6297(3)	3.63249(5)
b (Å)	5.2077(2)	5.2130(1)	5.2210(1)	5.2280(1)	5.2287(1)		5.2250(2)		
c (Å)	5.3171(2)	5.3249(2)	5.3387(1)	5.3540(1)	5.3667(1)	5.213(2)	5.3820(2)	5.2217(6)	5.22879(9)
β (deg)	99.224(2)	99.183(2)	99.116(2)	99.051(2)	99.004(2)		98.924(2)		
V (Å^3)	140.76(4)	141.35(3)	142.32(3)	143.47(3)	144.00(2)	68.67(5)	144.65(4)	68.80(2)	68.994(3)
Zr,Ce x	0.2746(3)	0.2748(6)	0.2751(10)	0.2751(6)	0.2742(7)		0.2731(10)		
y	0.0407(3)	0.0408(6)	0.0405(9)	0.0396(5)	0.0388(7)		0.0386(9)		
z	0.2078(2)	0.2085(5)	0.2085(8)	0.2089(5)	0.2096(6)		0.2104(8)		
β_{11}	0.0037(6)	0.0060(13)	0.0055(20)	0.0053(11)	0.0054(14)		0.0052(20)		
β_{22}	0.0032(6)	0.0024(13)	0.0018(20)	0.0027(12)	0.0030(15)		0.0046(23)		
β_{33}	0.0019(5)	0.0019(10)	0.0027(10)	0.0034(10)	0.0031(13)		0.0037(18)		
β_{12}	0.0002(5)	0.0011(11)	0.0017(17)	0.0019(10)	0.0012(12)		0.0014(15)		
β_{13}	0.0008(4)	0.0009(9)	0.0008(15)	0.0015(9)	0.0015(11)		0.0017(14)		
β_{23}	−0.0005(4)	0.0007(10)	0.0013(15)	0.0016(9)	0.0024(11)		0.0015(15)		
B (Å^2)	0.313	0.370	0.363	0.408	0.414	0.362	0.488	0.52(42)	0.40(31)
O(1) x	0.0705(3)	0.0701(7)	0.0694(12)	0.0673(7)	0.0655(9)		0.0621(11)		
y	0.3327(3)	0.3328(7)	0.3319(12)	0.3287(7)	0.3251(9)		0.3183(10)		
z	0.3447(3)	0.3452(6)	0.3471(9)	0.3495(6)	0.3533(7)	0.214(8)	0.3584(10)	0.2063(3)	0.2054(2)
β_{11}	0.0018(8)	0.0019(19)	0.0022(30)	0.0039(18)	0.0048(22)		0.0053(29)		
β_{22}	0.0035(7)	0.0063(16)	0.0076(26)	0.0068(16)	0.0062(20)		0.0057(27)		
β_{33}	0.0030(6)	0.0041(13)	0.0061(22)	0.0076(13)	0.0108(18)		0.0122(25)		
β_{12}	0.0008(6)	0.0011(13)	0.0010(19)	0.0020(11)	0.0018(13)		0.0015(18)		
β_{13}	−0.0035(5)	−0.0031(12)	−0.0016(19)	−0.0003(11)	0.0012(15)		0.0028(21)		
β_{23}	−0.0021(5)	−0.0033(10)	−0.0028(16)	−0.0028(9)	−0.0044(12)		−0.0042(15)		
B (Å^2)	0.328	0.470	0.592	0.682	0.808	0.533	0.856	0.66(33)	0.74(28)
O(2) x	0.4499(3)	0.4497(7)	0.4505(11)	0.4511(6)	0.4515(8)		0.4534(11)		
y	0.7588(3)	0.7578(7)	0.7573(11)	0.7561(6)	0.7551(8)		0.7540(11)		
z	0.4793(3)	0.4784(6)	0.4783(10)	0.4780(6)	0.4775(8)		0.4770(10)		
β_{11}	0.0032(8)	0.0033(18)	0.0030(28)	0.0033(16)	0.0035(19)		0.0039(24)		
β_{22}	0.0017(7)	0.0025(15)	0.0036(24)	0.0038(14)	0.0065(18)		0.0078(24)		
β_{33}	−0.0006(6)	0.0007(13)	0.0011(21)	0.0031(13)	0.0033(16)		0.0031(21)		
β_{12}	−0.0008(6)	−0.0006(13)	−0.0007(20)	−0.0018(12)	−0.0003(15)		−0.0006(19)		
β_{13}	0.0003(4)	−0.0001(9)	−0.0005(14)	0.0011(8)	0.0008(10)		0.0017(14)		
β_{23}	0.0020(4)	0.0011(10)	0.0006(16)	0.0012(10)	0.0004(13)		0.0016(18)		
B (Å^2)	0.151	0.232	0.282	0.366	0.484		0.532		
R_{wp} (%)	11.66	10.52	9.90	10.80	9.36		11.59		15.35
R_e (%)	11.74	9.76	6.95	10.07	7.42		9.65		7.08
R_{wp}/R_e	0.99	1.08	1.42	1.07	1.26		1.20		2.17

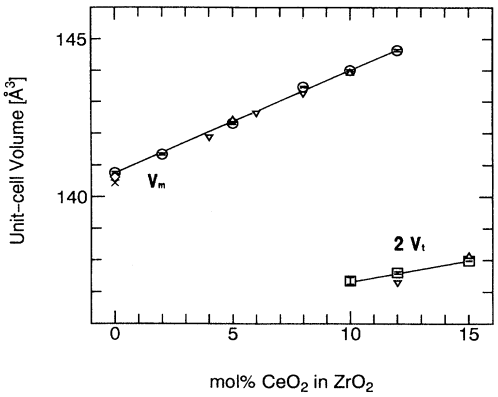

FIG. 5. Variation of the unit-cell volumes with the CeO_2 content: ○, present work (monoclinic phase); □, present work (tetragonal phase); △, Tani *et al.* (Ref. 4); ▽, Urabe *et al.* (Ref. 27); ◇, Frey *et al.* (Ref. 10); ×, Smith and Newkirk (Ref. 8).

$$\Delta K_{IC}=0.21 e^T E V_f \sqrt{h}\,/(1-\nu)\ ,$$

where e^T is the dilatational transformation strain that is equivalent to the cell volume ratio $V_m/2V_t$, and E, V_f, h, and ν are Young's modulus, the volume fraction of material susceptible to transformation, the transformation zone width, and Poisson's ratio, respectively. The cell volume ratios $V_m/2V_t$, which are important for the transformation toughening, are 1.050 and 1.051 in 10 and 12 mol % CeO_2 samples. These values are larger than 1.03 (Ref. 10) of undoped ZrO_2, but comparable to that in ZrO_2-X mol % $YO_{1.5}$ solid solution [e.g., $V_m/2V_t \approx 1.051$ (Ref. 21) for $X=4$]. Thus the transformation strain e^T is not responsible for the higher toughness of ZrO_2-CeO_2 than that of $YO_{1.5}$-doped ZrO_2, which should be mostly ascribed to the difference in the transformation plasticity.[16,25,26,42]

The b_m shows a small change with increasing of X, while a_m and c_m increase and β_m decreases with X (Figs. 3 and 4). This indicates that the unit-cell parameters of monoclinic ZrO_2 vary anisotropically with increasing of X. These changes are similar to those observed in cases both of thermal expansion[27,43,44] and doping of $YO_{1.5}$.[21] Patil and Subbarao[43] suggested that the temperature-induced anisotropy could be associated with the structure of ZrO_2 with a low symmetry and complex bonding with a considerable amount of covalent character.[8] As will be described later, we have obtained anisotropy of the thermal ellipsoid and complex positional changes of oxygen with X, which might also be associated with the anisotropy in the unit-cell parameter changes with X.

B. Positional parameters

The compositional dependence of the positional parameters is shown in Fig. 6, where these parameters are defined as the differences of atomic coordinates of the monoclinic phase from those in the tetragonal phase (its atomic coordinate z_t was fixed to be 0.2054 obtained for ZrO_2-15 mol % CeO_2). The positional parameter x of the

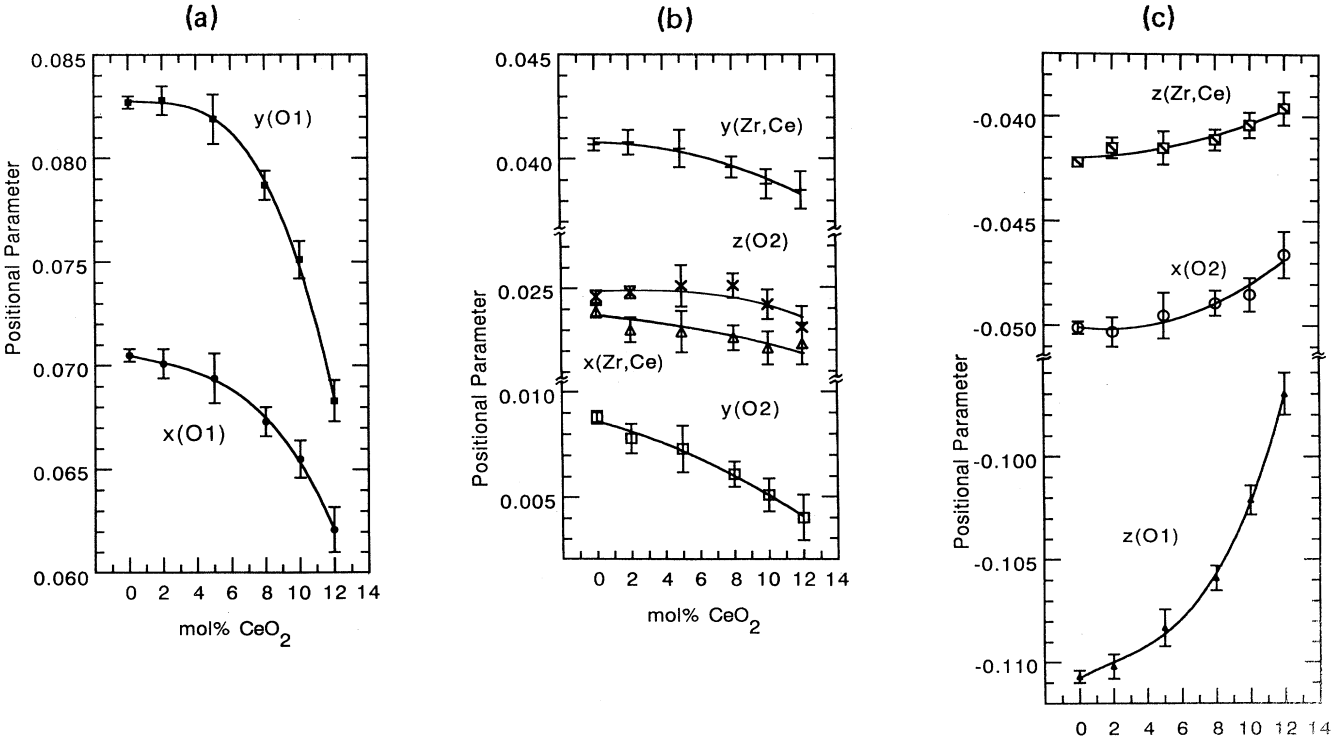

FIG. 6. Positional parameters of monoclinic ZrO_2-CeO_2, given as the difference from their values in the tetragonal phase: (a) y[O(1)] and x[O(1)]; (b) y(Zr,Ce), z[O(2)], x(Zr,Ce), and y[O(2)]; (c) z(Zr,Ce), x[O(2)], and z[O(1)].

cations (Zr,Ce), x(Zr,Ce), and y(Zr,Ce) decreases and z(Zr,Ce) increases with increasing of CeO_2 content X [Figs. 6(b) and 6(c)]. The positional parameters x[O(1)] and y[O(1)] decrease and z[O(1)] increases considerably with X [Figs. 6(a) and 6(c)]. The positional parameter x[O(2)] increases and y[O(2)] decreases with an increase of X [Figs. 6(c) and 6(b)]. The positional parameter z[O(2)] remains almost constant, but seems to decrease with X. Figure 6 indicates precursor phenomena for the monoclinic-to-tetragonal phase transition induced by CeO_2 doping, where the positional parameters of the monoclinic phase approach 0: those of the tetragonal phase.

It is interesting to compare the compositional dependence of the atomic positions of the ZrO_2-CeO_2 solid solutions with the temperature dependence in undoped ZrO_2. Around the temperature-induced monoclinic-tetragonal transition point in undoped ZrO_2, the atomic coordinates of the monoclinic phase did not always approach those of the tetragonal phase according to Frey and co-workers.[10,45] For example, x[O(1)] and y[O(1)] seem to increase with temperature around the transition temperature (Fig. 4 in Ref. 10). It is noteworthy that around the transition composition in CeO_2-doped ZrO_2 all positional parameters approach those of the tetragonal phase (Fig. 6). This suggests that the precursor phenomena observed in oxygen positions in the transition caused by the CeO_2 doping are different from those in the temperature-induced transition in undoped ZrO_2, although both seen in the unit-cell parameters are very similar.

The equivalent isotropic thermal parameters increase with an increase of CeO_2 content as shown in Fig. 7. The isotropic thermal parameter of O(1), B[O(1)], determined in the present study, has larger values than B[O(2)] and B(Zr,Ce) in the whole compositional region examined, which was also observed in undoped ZrO_2.[8,10] The largest thermal parameter B[O(1)] in all ions corresponds to the largest movement of O(1) during the monoclinic-tetragonal phase change shown by the dashed lines in Fig. 8(a). The increase of the disorder in the atomic positions with increasing of X is similar to that obtained by an extended x-ray-absorption fine-structure (EXAFS) study of zirconia-ceria solid solutions.[24]

Figure 8 shows the variation of the layer of ZrO_7 groups at $x=\frac{1}{4}$ projected on the (100) plane with an increase of the CeO_2 content X, where the position of the central cation is fixed for all compositions. With increasing of X, the oxygen ions approach the ideal positions in the tetragonal structure. The anisotropies of the thermal ellipsoids are similar to those for undoped ZrO_2 at high temperatures.[10,45] It is noteworthy that each O(1) ion moves with increasing of X in the direction of the major axis of its thermal ellipsoid. Each oxygen seems not to be located on the straight line between the ideal position in the tetragonal structure and that in the monoclinic undoped ZrO_2, but on a curved line shown by the dashed lines in Fig. 8(c). Complex potentials should exist for oxygen ions in the monoclinic zirconia materials, which yield various anisotropies for their thermal ellipsoids (Fig. 8), their complex movements with X, and the anisotropic changes in the unit-cell parameters with X.

This displacive phase transition induced by the CeO_2 doping shows a strong first-order character as seen from the steep changes in the unit-cell parameters at $X=10$ and 12 (Figs. 3–5). Such sudden changes are observed in the atomic positions during the phase transition (Figs. 6 and 8). However, the present study has also demonstrated the following characteristics: (1) The length of a_m approaches that of b_m with an increase of X (Fig. 3), (2) the β_m angle decreases with X (Fig. 4), and (3) all positional parameters of the monoclinic phase approach those of the tetragonal structure (Fig. 6). Some theoretical studies using appropriate potentials between ionic species are required to explain these complex structural changes.

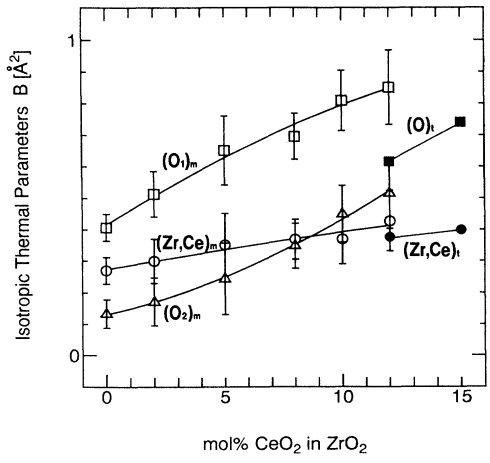

FIG. 7. Variation of the equivalent isotropic thermal parameters with CeO_2 content.

IV. CONCLUDING REMARKS

The present study has demonstrated various anisotropic and complicated aspects in the structural changes. First, the unit-cell parameters change anisotropically with an increase of CeO_2 content X: b_m shows a small change with X, while a_m and c_m increase and β_m decreases with X (Figs. 3 and 4) in a similar manner as the temperature dependence in undoped ZrO_2. Second, the thermal ellipsoids also show large anisotropies, which correlate strongly with the direction of the movement of each ionic species with X and during the phase transition.

This displacive phase transition induced by the CeO_2 doping shows a strong first-order character as seen from the steep changes in the unit-cell parameters and in the atomic positions during the phase transition. The present study has also demonstrated that (1) the length of a_m approaches that of b_m with an increase of X, (2) the β_m angle decreases with X, and (3) all positional parameters of the monoclinic phase approach those of the tetragonal structure.

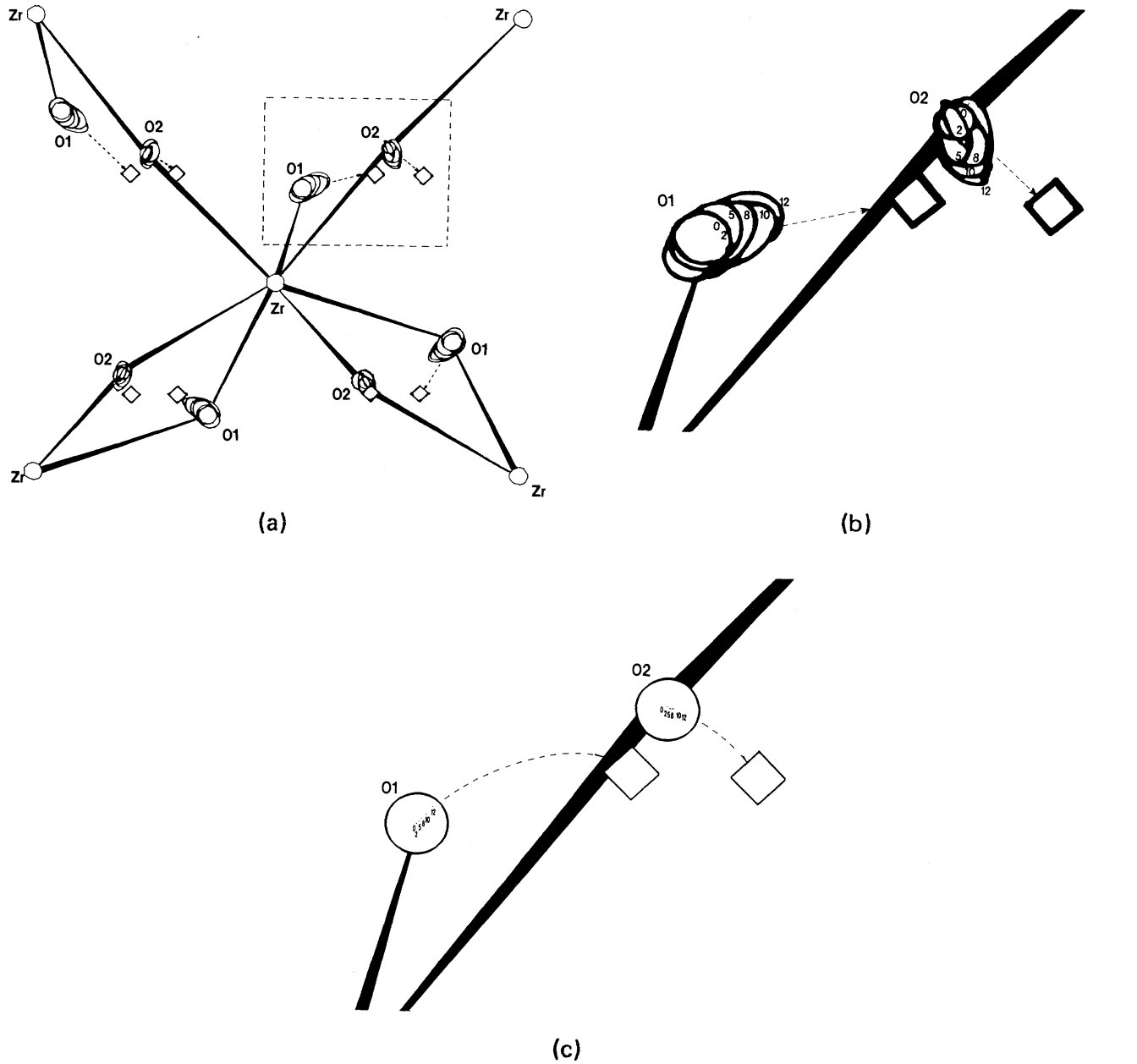

FIG. 8. (a) The variation of the layer of ZrO_7 groups at $x = \frac{1}{4}$ projected on the (100) plane with CeO_2 content. The variation of one O(1) and one O(2) (b) with and (c) without thermal ellipsoids. Each point with a number X in (b) and (c) denotes the ellipsoid or the position of an oxygen in the ZrO_2-X mol % CeO_2 sample. ◇ indicates the ideal position of oxygen in the tetragonal structure of the 15 mol % CeO_2 sample.

ACKNOWLEDGMENTS

We would like to express our thanks to Y. Shimojyo for the neutron-diffraction measurements. Support from the Department of Research Reactor of JAERI is acknowledged. Support for M. Yashima was partly provided by Shôrei-kenkyu Grant-in-Aid No. 06750688 for Fundamental Research from the Ministry of Education, Science and Culture. Support for M. Yoshimura was provided by the Mitsubishi foundation. The Rietveld refinements were performed using a UNIX computer in the Computer Center, Tokyo Institute of Technology with the help of Nakamura and Itoh's laboratory.

[1]M. Yashima, H. Arashi, M. Kakihana, and M. Yoshimura, J. Am. Ceram. Soc. **77**, 1067 (1994).
[2]M. Yashima, H. Takashina, M. Kakihana, and M. Yoshimura, J. Am. Ceram. Soc. **77**, 1869 (1994).
[3]Y. Du, M. Yashima, T. Koura, M. Kakihana, and M. Yoshimura, Scr. Metall. Mater. **31**, 327 (1994).
[4]E. Tani, M. Yoshimura, and S. Sōmiya, J. Am. Ceram. Soc. **66**, 506 (1983).
[5]M. Yoshimura, E. Tani, and S. Sōmiya, Solid State Ion. **3/4**, 477 (1981).
[6]M. Yoshimura, Am. Ceram. Soc. Bull. **67**, 1950 (1988).
[7]J. D. McCullough and K. N. Trueblood, Acta Crystallogr. **12**, 507 (1959).
[8]D. K. Smith and H. Newkirk, Acta Crystallogr. **18**, 983 (1965).
[9]G. Teufer, Acta Crystallogr. **15**, 1187 (1962).
[10]F. Frey, H. Boysen, and T. Vogt, Acta Crystallogr. B **46**, 724 (1990).
[11]E. C. Subbarao, H. S. Maiti, and K. K. Srivastava, Phys. Status Solidi A **21**, 9 (1974).
[12]P. Aldebert and J.-P. Traverse, J. Am. Ceram. Soc. **68**, 34 (1985).
[13]K. Tsukuma and M. Shimada, J. Mater. Sci. **20**, 1178 (1984).
[14]K. Tsukuma, Am. Ceram. Soc. Bull. **65**, 1368 (1986).
[15]I. Nettleship and R. Stevens, Int. J. High Technol. Ceram. **3**, 1 (1987).
[16]L. R. F. Rose and M. V. Swain, Acta Metall. **36**, 955 (1988).
[17]M. Yashima, K. Morimoto, N. Ishizawa, and M. Yoshimura, J. Am. Ceram. Soc. **76**, 1745 (1993).
[18]M. Yashima, K. Morimoto, N. Ishizawa, and M. Yoshimura, J. Am. Ceram. Soc. **76**, 2865 (1993).
[19]R. C. Garvie, R. H. Hannink, and R. T. Pascoe, Nature **258**, 703 (1975).
[20]A. G. Evans, in *Science and Technology of Zirconia II,* edited by N. Claussen, M. Rühle, and A. H. Heuer, Advances in Ceramics Vol. 12 (American Ceramic Society, Westerville, OH, 1984), pp. 193–212.
[21]H. Toraya, J. Am. Ceram. Soc. **72**, 662 (1989).
[22]N. Nakanishi and T. Shigematsu, Mater. Trans. Jpn. Inst. Metals **32**, 778 (1991).
[23]P. Li, I.-W. Chen, and J. E. Penner-Hahn, Phys. Rev. B **48**, 10053 (1993); **48**, 10074 (1993); **48**, 10082 (1993).
[24]P. Li, I.-W. Chen, and J. E. Penner-Hahn, J. Am. Ceram. Soc. **77**, 1281 (1994).
[25]P. E. Reyes-Morel and I.-W. Chen, J. Am. Ceram. Soc. **71**, 343 (1988).
[26]P. E. Reyes-Morel, J.-S. Cherng, and I.-W. Chen, J. Am. Ceram. Soc. **71**, 648 (1988).
[27]K. Urabe, K. Ogata, H. Ikawa, and S. Udagawa, Mater. Sci. Forum **34-36**, 147 (1988).
[28]X. L. Zhe, B. Li, S. H. Zhang, and T. M. Wang, Phys. Status Solidi A **136**, K9 (1993).
[29]G. X. Cheng and X. K. Zhang, Wuli Xuebao **39**, 1344 (1990).
[30]R. H. J. Hannink and M. V. Swain, J. Am. Ceram. Soc. **72**, 90 (1989).
[31]Y. Kubota, M. Ashizuka, and H. Hokazono, J. Ceram. Soc. Jpn. **102**, 175 (1994).
[32]H. M. Rietveld, J. Appl. Crystallogr. **2**, 65 (1969).
[33]F. Izumi, J. Crystallogr. Soc. Jpn. **27**, 23 (1985).
[34]F. Izumi, in *The Rietveld Method,* edited by R. A. Young (Oxford University Press, New York, 1993), pp. 236–253.
[35]Y. Morii, K. Fuchizaki, and S. Funahashi, in *Proceedings of the Fourth International Symposium on Advanced Nuclear Energy Research: Roles and Direction of Material Science in Nuclear Technology,* edited by Japan Atomic Energy Research Institute (Japan Atomic Energy Research Institute, Tokai Ibaraki, Japan, 1992), pp. 280–284.
[36]Y. Morii, J. Crystallogr. Soc. Jpn. **34**, 62 (1992).
[37]H. Toraya, J. Appl. Crytallogr. **19**, 440 (1986); H. Toraya, in *The Rietveld Method,* edited by R. A. Young (Oxford University Press, New York, 1993), pp. 254–275.
[38]T. Funahahi, Y. Ito, and H. Yoshizawa, Bull. Phys. Soc. Jpn. **46**, 1003 (1991).
[39]M. Yashima, S. Sasaki, M. Kakihana, Y. Yamaguchi, H. Arashi, and M. Yoshimura, Acta Crystallogr. B **50**, 663 (1994).
[40]R. D. Shannon, Acta Crystallogr. A **32**, 751 (1976).
[41]M. Yashima, N. Ishizawa, and M. Yoshimura, J. Am. Ceram. Soc. **75**, 1550 (1992).
[42]G. Grathrohl and T. Liu, J. Am. Ceram. Soc. **74**, 3028 (1991).
[43]R. N. Patil and E. C. Subbarao, J. Appl. Crystallogr. **2**, 281 (1969).
[44]R. Ruh, G. W. Hollenberg, S. R. Skaggs, S. D. Stoddard, F. D. Gac, and E. G. Charles, Am. Ceram. Soc. Bull. **60**, 504 (1981).
[45]H. Boysen, F. Frey, and T. Vogt, Acta Crystallogr. B **47**, 881 (1991).
[46]R. A. Young, E. Prince, and R. A. Sparks, J. Appl. Crystallogr. **15**, 357 (1982).